NURETH14-79

CORRELATION BETWEEN FLOW ACCELERATED CORROSION AND WALL SHEAR STRESS DOWNSTREAM FROM AN ORIFICE

Y. UTANOHARA¹, A. NAKAMURA¹, Y. NAGAYA¹ and M. MURASE¹

¹ Institute of Nuclear Safety System, Inc. Fukui, Japan utanohara@inss.co.jp, a-naka@inss.co.jp, nagaya.yukinori@inss.co.jp, murase@inss.co.jp

Abstract

To evaluate the effects of flow field on FAC, orifice flow was measured using LDV and simulated by LES. FAC rate was also measured in a test loop. The LDV measurements indicated the flow structure did not depend on the flow velocity. Flow field predicted by RANS and LES agreed well with LDV data. The metal loss increased linearly with time downstream from the orifice but gradually decreased upstream. FAC rate increased as velocity increased. FAC rate predicted by LES had a clear relationship with the predicted RMS of wall shear stress.

Introduction

Flow accelerated corrosion (FAC) is an important issue for aging power plants. FAC causes thinning of the pipe wall, and occasionally a piping rupture accident has occurred. The Japanese Society of Mechanical Engineers published a guideline on pipe wall thinning management in 2005 [1]. FAC and liquid droplet impingement (LDI) were treated in the guideline and since then, thinning of pipe wall thickness has been managed based on non-destructive inspection of pipe wall thickness and evaluation of remaining lifetime.

Some experiments on FAC have been conducted, and effects of temperature [2], pH [3], dissolved oxygen [4] and velocity [2][5] on corrosion rates were reported. Keller [6] reported geometry factors of pipe elements. Some prediction models and correlations to evaluate corrosion rates [7]-[9] have been proposed, but the predicted values have large deviations from the plant data. Most reports have focused on effects of water chemistry and mean cross-sectional velocity on FAC rates and only a few reports evaluated effects of the local flow field and distribution of FAC rates. In a power plant, distribution of wall thickness is measured to evaluate remaining lifetime. Therefore, predicting the distribution of FAC rates is useful for planning non-destructive inspection of pipe wall thickness.

Computational fluid dynamics (CFD) is a useful tool to investigate the relationship between local flow field and FAC rate. There have been many CFD studies to clarify the effect of local flow field on FAC [10] [11], but details of the relationship are still not well understood.

In order to evaluate the effects of local flow field on the distribution of FAC rate, the authors have measured FAC rate of an orifice flow in a high-temperature water test loop [12]. In addition, the orifice flow field has been simulated numerically and compared with the measured velocity profiles obtained by laser Doppler velocimetry (LDV) and particle image

velocimetry (PIV) to validate the numerical simulation [12][13]. Measured FAC rate was compared with the predicted wall shear stress, which was employed as an evaluation parameter of FAC. According to the results, the downstream/upstream ratio of the wall shear stress predicted by the steady Reynolds averaged Navier-Stokes (RANS) simulation agreed well with the ratio of FAC rate at 1D downstream from the orifice. However, the ratio of the wall shear stress underestimated the ratio of FAC rate around the reattachment point. To examine the reason for the underestimation, large eddy simulation (LES) was carried out [13]. The LES results indicated instantaneous wall shear stresses were not low and often changed their directions around the reattachment point. Hence, when wall shear stresses were timeaveraged, the value became low, because the time-averaging procedure cancelled out fluctuating wall shear stresses. The result of the steady RANS also has a time-averaged characteristic. This might be why the wall shear stress predicted by the steady RANS became low and underestimated the ratio of FAC rate. On the contrary, the root mean square (RMS) of wall shear stresses by LES was not low around the reattachment point. The RMS value might be better than the time-averaged value for comparison with FAC rate. The velocity profiles predicted by LES, however, did not agreed well with LDV data. One of the possible reasons was the computational domain, for which one quarter of the cross section was used to save computational time; it seemed unable to simulate asymmetric flow downstream from the orifice.

In this paper, LES of the full pipe geometry was carried out to improve the prediction of the flow field and mitigate underestimation of FAC rate around the reattachment point. The orifice flow field was additionally measured by LDV to understand the flow field in more detail. FAC rate was also measured and the dependency of flow velocity on it was investigated. Measured FAC rate was compared with the predicted wall shear stress.

1. Experimental methods

1.1 Evaluation parameter of the FAC rate

In FAC, iron ions from carbon steel dissolve into a concentration boundary layer where their transport to bulk fluid is accelerated by high velocity flow and turbulence. Diffusion flux of iron ions J is expressed as follows:

$$J = k_e (C_w - C_\infty) \tag{1}$$

where k_e is mass transfer coefficient and C_w and C_∞ are concentrations of iron ions at an oxide-solution interface and bulk fluid, respectively. Many analogies have been proposed for the relationship between momentum and mass transfer. One is the Chilton-Colburn analogy:

$$j_D = \frac{C_f}{2} \tag{2}$$

where j_D is the j-factor for mass transfer and C_f is the skin-friction coefficient. They are expressed as:

$$j_{D} = \frac{Sh}{ReSc^{1/3}} = \frac{k_{e}}{U_{ave}}Sc^{2/3}, \qquad C_{f} = \frac{\tau_{w}}{\frac{1}{2}\rho U_{ave}^{2}}$$
(3)

where U_{ave} is mean cross-sectional velocity in the case of pipe flow, τ_w is wall shear stress and ρ is density. Reynolds number Re, Schmidt number Sc and Sherwood number Sh are described as follows:

$$Re = \frac{U_{ave}D}{V}, \quad Sc = \frac{V}{\Gamma}, \quad Sh = \frac{k_eD}{\Gamma}$$
 (4)

where D is pipe diameter, v is kinematic viscosity, and Γ is mass diffusion coefficient. Hence mass transfer coefficient k_e can be derived as

$$k_e = \frac{\tau_w}{\rho U_{ove}} Sc^{-2/3} \,. \tag{5}$$

Based on this relationship, the authors thought that FAC rate could be evaluated by the wall shear stress.

1.2 Test loop

Figure 1 shows the test loop which consists of a hot water tank and loop, pressure control system with nitrogen gas, feed water system with degasification unit, water quality control system, and measurement system for water chemical parameters. The test loop could be operated up to the pressure of 2.0 MPa and temperature of 473 K (200 °C). The system pressure was automatically controlled by nitrogen gas, and the loop temperature was automatically controlled by heater power. During operation at a constant temperature, the heat generated by the recirculation pump was cooled by a cooler. The inner diameter of the test section was D = 50 mm. Concentration of dissolved oxygen of the feed water and the test loop could be decreased by the degasification unit at room temperature before heating. Additionally, to decrease oxygen concentration, hydrazine solution can be injected into the test loop while for control of pH, sulfuric acid solution and ammonia solution can be used; however, these were not done in the present study.

During experiments, pressure of the hot water tank, temperature and flow rate in the loop were measured. In the measurement system for water quality, dissolved oxygen, conductivity and pH were measured at low pressure and room temperature. In addition, feed water was sampled directly from the test loop taking care not to expose the sample to air, and pH and iron concentration were measured using handy-type measuring instruments.

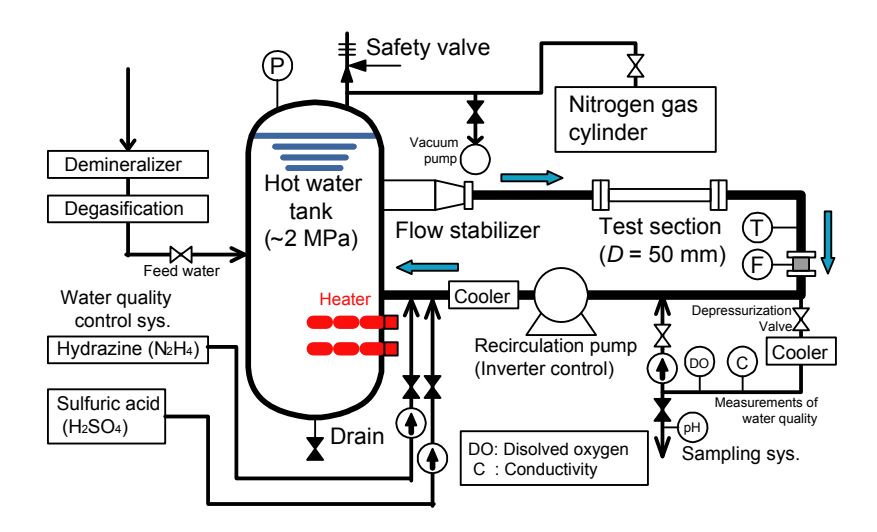


Figure 1 Test loop.

1.3 Measurement method of velocity profile

Velocity profile downstream from an orifice was measured using an LDV system (KANOMAX, Smart LDV, Model 8739-S). Figure 2 shows a schematic diagram of a transparent acrylic resin test section; the pipe diameter was 50 mm and the orifice diameter was 24.3 mm, hence the diameter ratio was about 0.5. A water jacket surrounded the pipe to minimize refractions of the laser at the boundary. The temperature of the working fluid (water) was room temperature (about 20 °C) and flow velocity was set to conditions shown in Table 1. Nylon resin particles, 4.1 µm mean diameter and 1020 kg/m³ density, were used. The number of samplings to obtain the mean velocity by LDV was about 30,000.

Table 1 Flow velocity conditions of LDV

J					
Flow rate [m ³ /h]	Mean cross-sectional velocity U_{ave} [m/s]	$Re=U_{ave}D/v$			
3.3	0.47	2.3×10^4			
11	1.6	7.8×10^4			
17	2.4	1.2×10^{5}			

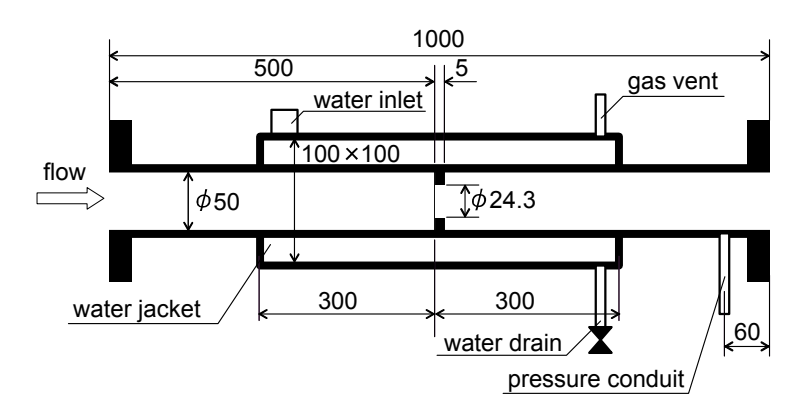


Figure 2 Test section for LDV (unit: mm).

1.4 Measurement method of FAC

Figure 3 and Figure 4 show the test section and corrosion sensor for FAC rate measurement. The SUS 304 pipe was 50 mm in inner diameter and had an orifice diameter of 24.3 mm. Corrosion sensors made of carbon steel plate (STPT 42: Ni, 0.02 wt. %; Cr, 0.04 wt. %; Mo, 0.01 wt. %) were insulated from the SUS 304 pipe with a resin covering and implanted in the pipe wall so that one surface of the plates was exposed to the fluid (hot water) flowing in the pipe as shown in Figure 4. The inner surface of the test section was bored using a boring machine to remove undesirable bumps between corrosion sensors and the pipe wall and get a tight fit. Four sensors were installed in the circumferential direction at 1D and 2D downstream from the orifice, two were at 3D and 4D downstream, and four were at 3D upstream. The FAC rate was measured using the electric resistance method. The resistance of the sensor plate R is expressed as:

$$R = \rho_e \frac{L}{S} = \rho_e \frac{L}{dw} \tag{6}$$

where ρ_e is electric resistivity, and L, S, d and w are length, cross-sectional area, thickness and width of the sensor plate, respectively. To compensate for the temperature change of resistance, a reference plate of the same material and same size as the exposed plate was used. Because the electric resistivities ρ_e of the exposed and reference plate are the same for the same temperature and L and w do not change during an experiment, the thickness of the exposure plate d_{exp} is expressed as

$$d_{exp} = d_{ref} \frac{R_{ref}}{R_{exp}} \tag{7}$$

where suffixes of exp and ref denote the values of exposed and reference plates, respectively. FAC rate can be obtained by measuring R_{exp} and R_{ref} at regular time intervals.

The experimental conditions are shown in Table 2. Two experimental runs, Run 1 and Run 2, were conducted to clarify effect of flow velocity on FAC rate. Flow velocity was changed from 1.4 to 5 m/s during Run 1 and from 2.1 to 3.5 m/s during Run 2. Water temperature was controlled around 150 °C. Dissolved oxygen was almost always under 0.1 ppb and pH at room temperature was around 6.

Table 2 Experimental conditions of FAC

	Run 1		Run 2	
Mean cross-sectional velocity U_{ave} [m/s]	1.4	5.0	2.1	→ 3.5
Re (150°C, 1.5 MPa)	3.6×10 ⁵	1.2×10 ⁶	5.3×10 ⁵	8.9×10 ⁵
Temperature [°C]	149.8			
Dissolved oxygen [ppb]	0.1			
pH at room temperature	5.8 - 6.2			

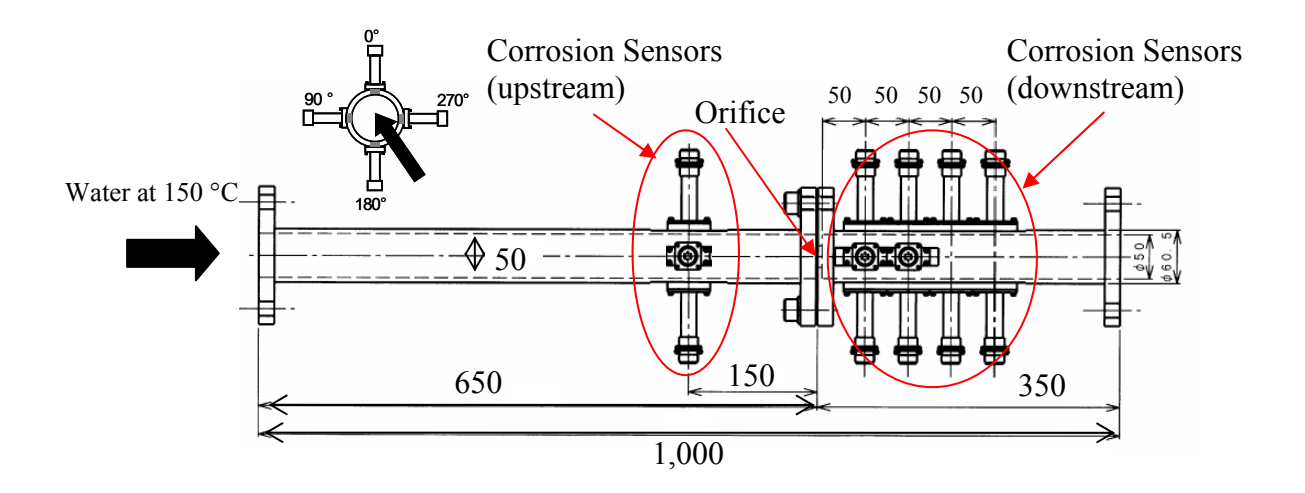


Figure 3 Test section for measurements of FAC rate (unit: mm).

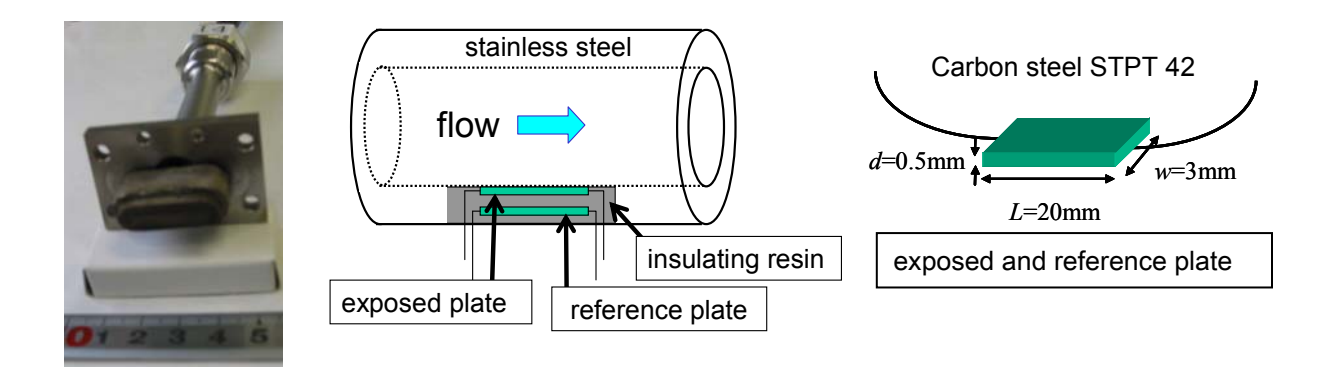


Figure 4 Corrosion sensor.

2. Numerical simulations

An orifice flow was simulated using the commercial CFD software FLUENT 6.3.26. Details of simulation conditions are shown in Table 3. Two types of simulations were carried out; the steady RANS simulation using the low Reynolds number k- ε AKN model (LRKE) and the transient simulation using LES. The computational grid shown in Figure 5 was used in both simulations. Hexahedral mesh and O-grid topology were used to fit the surface of the pipe wall. Mesh resolution was determined by reference to Eguchi *et al.*[14]. On the surface of the wall downstream from the orifice, the normalized radial mesh width was set to $y^+ < 1$ (LRKE) and $y^+ < 3$ (LES). The length of the computational domain was about 2D upstream and 7D downstream from the orifice. Statistics such as time-averaged value were derived from 15,000 to 50,000 time steps.

Table 3 Simulation conditions

Fluid	Water (25°C)				
	Density	997 kg/m³			
	Viscosity	8.899×10 ⁻⁴ Pa s			
Turbulence model		Low Re k - $arepsilon$ (AKN model)	LES (Smagorinsky)		
Time integration			2nd order backward Euler method, $\Delta t = 3.33 \times 10^{-5}$ s		
Convection term		2nd order upwind	Bounded central differencing		
Boundary conditions	Inlet	$U_{ave} = 0.453 \text{ m/s}$ ($Re = 2.25 \times 10^4$)			
		Turbulent intensity: 5% Turbulent viscosity ratio: 10	The 1/7th power law with fluctuation (spectral synthesizer)		
	Outlet	Neumann condition $\partial/\partial x = 0$ at outlet boundary	Pressure boundary (average static pressure 0 Pa)		
	Wall	Non-slip			
Computational domain		Upstream 2D, downstream 7D			
The number of meshes	4,096,800 (Cross sections:15,840)				

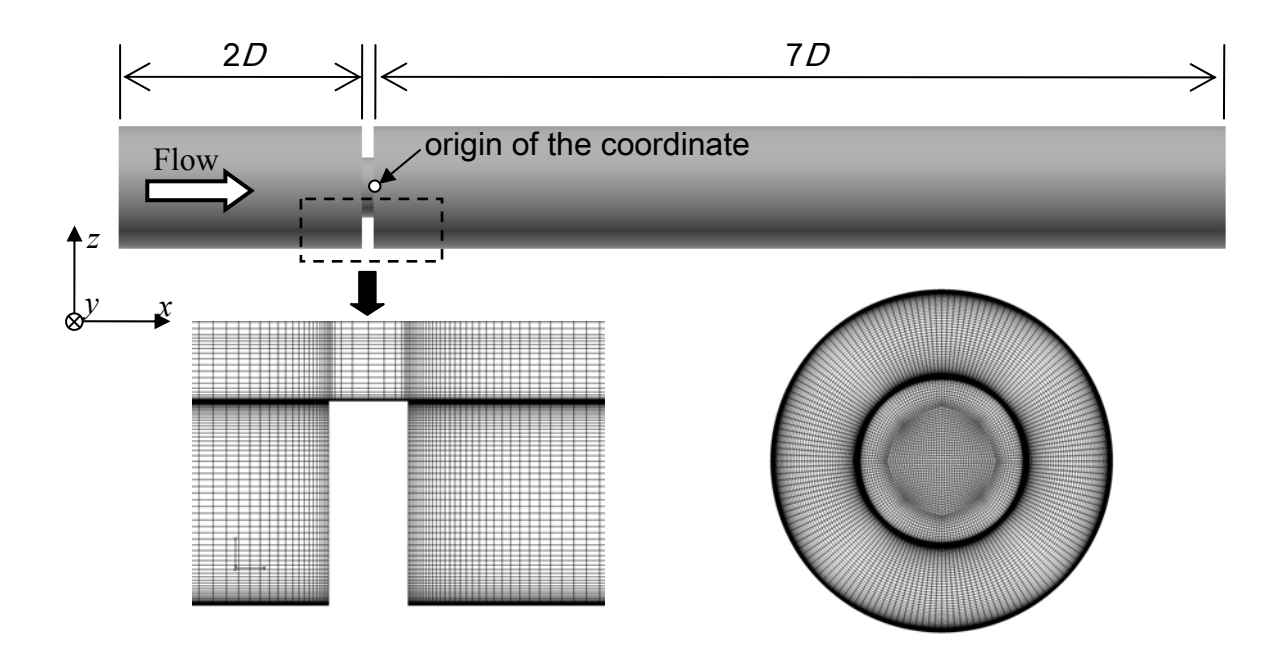


Figure 5 Computational domain and grid.

3. Results and discussion

3.1 Structure of flow field

As shown in Figure 5, the x, y and z-coordinates were defined to be the longitudinal, spanwise and vertical directions, respectively, and the origin of the coordinate system was set at the center of the outlet cross section of the orifice.

Figure 6 shows the time-averaged axial velocity profiles at 1D to 4D downstream from the orifice measured by LDV and simulated by RANS and LES. They were normalized by the mean cross-sectional velocity U_{ave} . Despite the difference in U_{ave} , velocity profiles measured by LDV at $U_{ave} = 0.47$ and 2.4 m/s, agreed well with each other when they were normalized. Hence, the flow structure downstream from the orifice does not depend on the flow velocity in the range of $Re = 2.3 \times 10^4$ to 1.2×10^5 , and probably in a wider range than that.

Figure 7 shows axial velocity profiles 1 mm from the wall downstream from the orifice along the axial length x from the orifice. These profiles also did not depend on flow velocity. The flow was reversed in the separation region and the reattachment point was presumed to be around 2.5D downstream from the orifice based on this velocity profile. Flow velocity reached the maximum of $u/U_{ave} = 1.0$ at around 1D.

Predicted velocity profiles are also shown in Figure 6 and Figure 7. In Figure 6, both LRKE and LES agreed well with LDV data, but LES slightly underestimated LDV data around the center of the pipe at 2D downstream. In the case of profiles near the wall in Figure 7, LES predicted LDV data quantitatively with slight deviation. As observed above, numerical simulations, particularly LES, predicted well the flow field downstream from the orifice. Hence, wall shear stress was also expected to be predicted well.

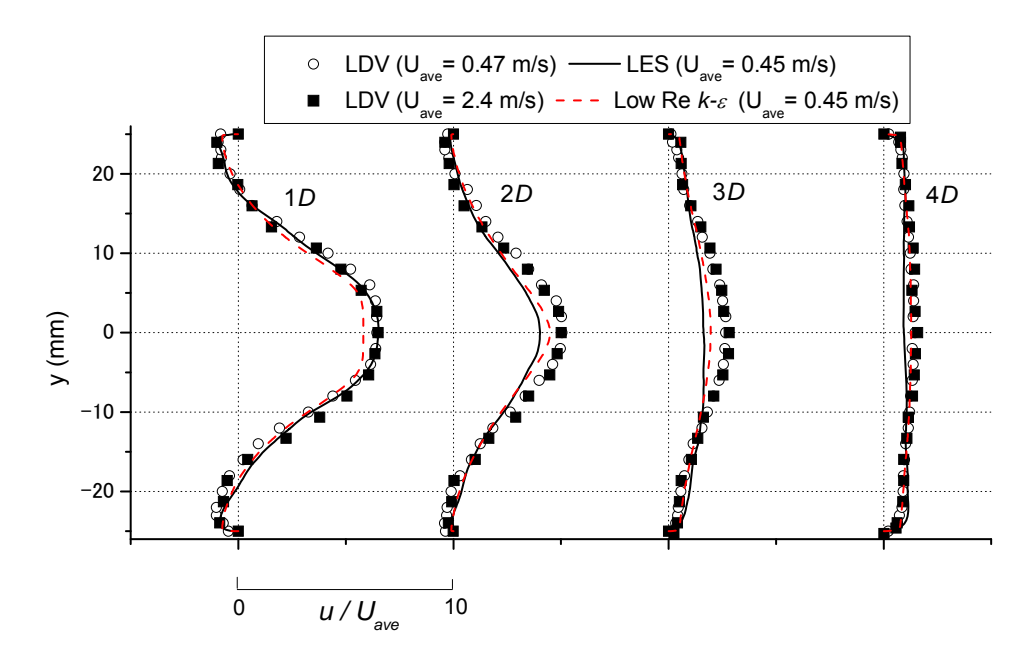


Figure 6 Axial velocity profiles downstream from the orifice.

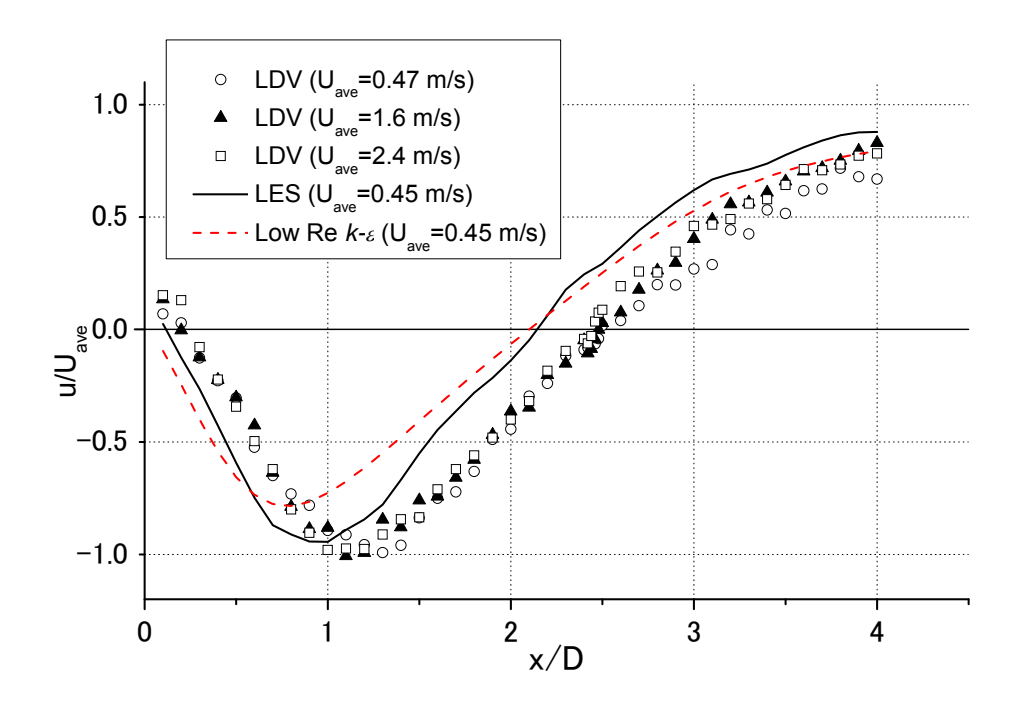


Figure 7 Axial velocity profiles near the wall (y = 1 mm from the wall).

3.2 Results of FAC rate measurement

Figure 8 shows time histories of metal loss of corrosion sensors at 2D downstream and 3D upstream from the orifice as obtained in Run 1. At 2D downstream, the metal loss increased linearly with time. No difference of metal loss was observed at two circumferential angles 0 and 180 deg. In Run 1, when mean cross-sectional velocity U_{ave} was changed from 1.4 m/s to 5.0 m/s at 117 h, the gradient of the metal loss curve increased sharply. On the other hand, metal loss rate at 3D upstream gradually slowed with time. In addition, influence of flow velocity change was little and the gradual decrease of the metal loss rate continued. The possible reason of this difference was the difference of the mass transfer coefficient near the wall. According to the experimental results by Bignold et al. [5], metal loss rate of mild steel was linear with time. However, in the case of 1% Cr content steel, metal loss rate was initially rapid and quickly decreased to a low metal loss rate during the initial formation of the oxide film from an essentially oxide-free surface. In this case, the solubility of the Cr seems to affect the growth rate of the oxide film. A similar situation might occur upstream from the orifice in this study, namely, the low mass transfer coefficient near the wall led to the growth of oxide film and the decrease of metal loss rate. This meant that even if the corrosion sensor was at the downstream, the low mass transfer coefficient at low flow velocity might cause gradual decrease of metal loss rate.

Figure 9 shows the distribution of the FAC rate downstream from the orifice. The qualitative tendency of the distribution was the same for different flow velocities; maximum FAC rate appeared at 1D or 2D, and gradually decreased downstream at 3D and 4D. FAC rate increased as flow velocity increased.

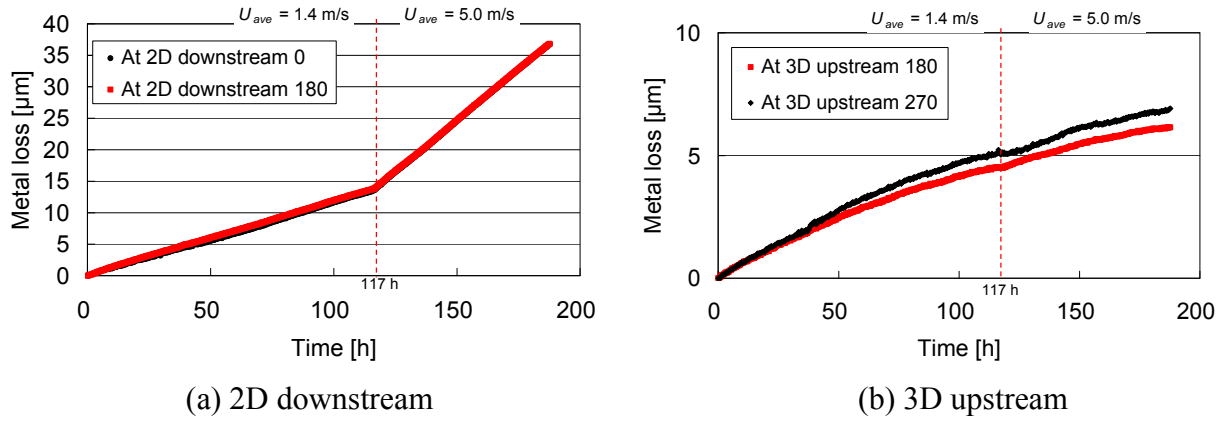


Figure 8 Time histories of metal loss at 2D downstream and 3D upstream in Run 1.

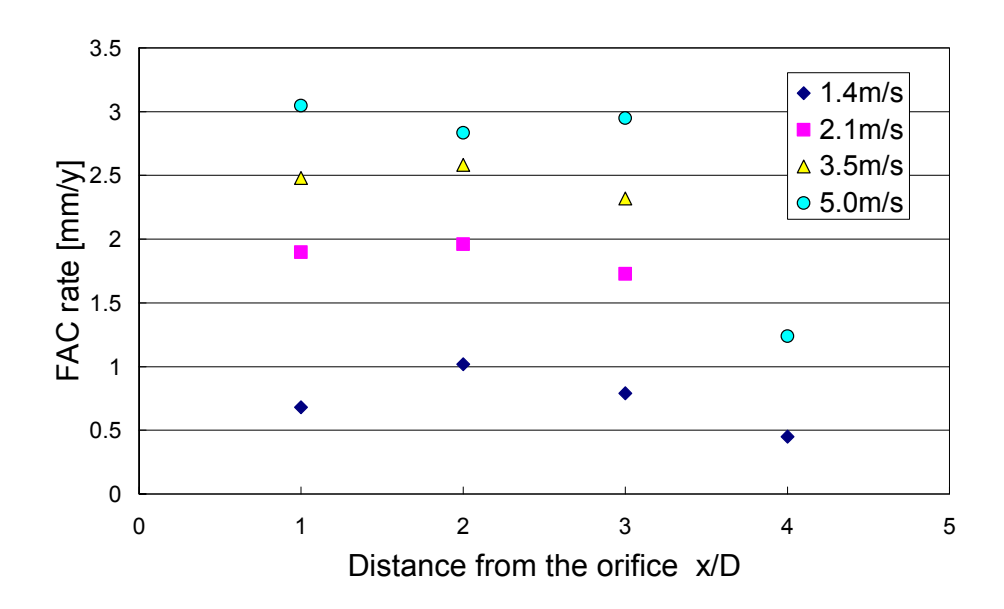


Figure 9 Distribution of FAC rate downstream from the orifice.

3.3 Predicted wall shear stress

Figure 10 shows wall shear stress τ_w predicted by LES and LRKE. LES results are time-averaged and RMS values. All values in Figure 10 were circumferentially-averaged. τ_w is the component parallel to the wall surface and was given as:

$$\tau_{w} = \sqrt{\tau_{wx} + \tau_{w\theta}} . \tag{8}$$

where τ_{wx} and $\tau_{w\theta}$ are the streamwise and circumferential components, respectively. RMS values were derived from:

$$\tau_{w,RMS} = \sqrt{\overline{\tau_w^2}} \ . \tag{9}$$

It should be noted that RMS values were not the root mean square of the fluctuation values, but involved time-averaged and fluctuated values. Time-averaged wall shear stress $\tau_{w,ave}$ of LES had a maximum value of 5 Pa at 1D and gradually decreased to almost 0 around the reattachment point 2.5D, then increased to 2 Pa. The predicted τ_w of LRKE was also the same profile as $\tau_{w,ave}$ by LES, because the steady RANS simulation predicted the time-averaged flow field. On the other hand, $\tau_{w,RMS}$ had a significant value around the reattachment point, because it involved time-averaged and fluctuated values.

The authors investigated the reason for the difference between time-averaged and RMS wall shear stress around the reattachment point [13] and found that the direction of instantaneous wall shear stress around the reattachment point fluctuated at any time. Hence, the time-averaging operation canceled out the wall shear stress of the opposite directions and a low value was derived even if instantaneous wall shear stress was a large value. As mentioned in Section 1, FAC rate had a significant value around the reattachment point and time-averaged wall shear stress underestimated the FAC rate. RMS wall shear stress $\tau_{w,RMS}$ was, therefore, used to compare FAC rate downstream from the orifice.

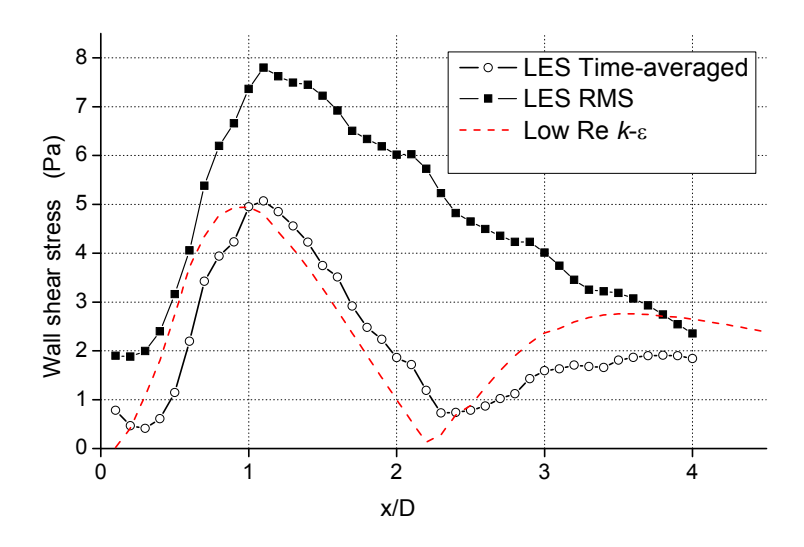


Figure 10 Predicted wall shear stress predicted by LES and LRKE.

3.4 Correlation between FAC rate and predicted wall shear stress

Figure 11 shows the correlation between FAC rate and the RMS wall shear stress $\tau_{w,RMS}$ predicted by LES. $\tau_{w,RMS}$ values were converted once to the skin-friction coefficients C_f (Eq.(3)) and again converted to the wall shear stress of experimental conditions ($U_{ave} = 1.4$ -5.0 m/s, density under 150 °C and 1.5 MPa). As shown in the figure, there was a clear relationship between FAC rate and the RMS wall shear stress. This indicates that FAC rate can be described as a function of the wall shear stress. However, the numbers of data are still not sufficient and the tendency of higher velocities case is not clear yet.

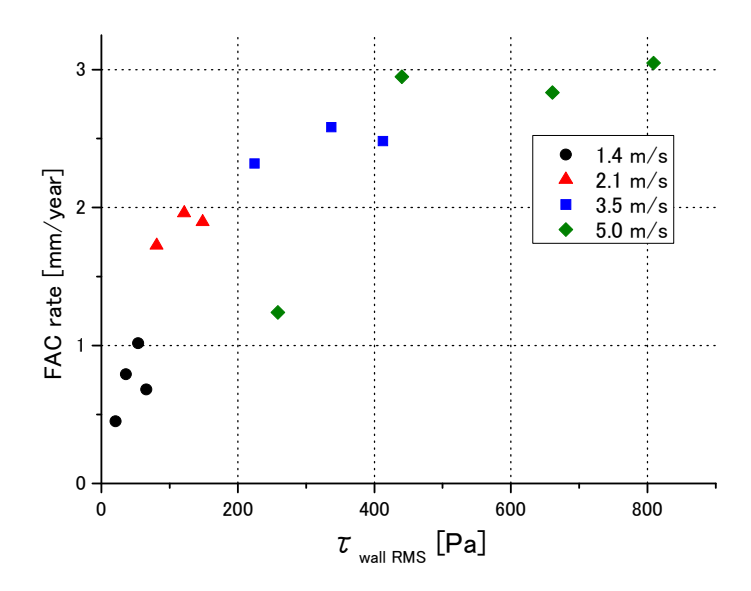


Figure 11 FAC rate and wall shear stress by LES.

4. Conclusions

- (1) The flow structure downstream from the orifice did not depend on the flow velocity in the range of $Re = 2.3 \times 10^4$ to 1.2×10^5 , and probably in a wider range than that. When the orifice-pipe diameter ratio was about 0.5, the reattachment point was around 2.5D downstream from the orifice. The maximum velocity near the wall in the separation region was almost equivalent to the mean cross-sectional velocity at 1D.
- (2) RMS wall shear stress predicted by LES had its maximum value around 1D and gradually decreased downstream, while the time-averaged wall shear stress rapidly decreased at distances greater than 1D downstream and became the minimum value around the reattachment point.
- (3) The tendency of FAC was different downstream and upstream from the orifice. The metal loss increased linearly with time downstream although metal loss rate gradually decreased with time upstream. The possible reason of this difference was the difference of the mass transfer coefficient near the wall.
- (4) There was a clear relationship between FAC rate and the predicted RMS of wall shear stress by LES.

5. References

- [1] Japanese Society of Mechanical Engineers, "Codes for power generation facilities Rules on pipe wall thinning management –", JSME S CA1-2005, 2005.
- [2] H. G. Heitmann and P. Schub, "Initial experience gained with a high pH value in the secondary system of PWRs", <u>Proc. of the Third Meeting on Water Chemistry of Nuclear Reactors</u>, British Nuclear Engineering Society, London, UK, 1983 Oct. 10-14, pp. 243-252.

- [3] H. G. Heitmann and W. Kastner, "Erosionskorrosion in wasser-dampfkreisläufen ursachen und gegenmassnahmen", *VGB-Kraftwerkstechnik*, Vol. 62, No. 3, 1982, pp.211-219.
- [4] O. de Bouvier, M. Bouchacourt and K. Fruzzetti, "Redox condition effect on flow accelerated corrosion: influence of hydrazine and oxygen", <u>Proc. of International Conference on Water Chemistry in Nuclear Reactor Systems</u>, 117, Avignon, France, 2002 Apr. 22-26.
- [5] G. J. Bignold, C. H. De Whalley, K. Garbett and I. S. Woolsey, "Mechanistic aspects of erosion-corrosion under boiler feedwater conditions", <u>Proc. of the Third Meeting on Water Chemistry of Nuclear Reactors</u>, British Nuclear Engineering Society, London, UK, 1983 Oct. 10-14, pp. 219-226
- [6] H. Keller, "Erosionskorrosion an Nassdampfturbien", *VGB-Kraftwerkstechnik* Vol. 54, No. 5, 1974, pp. 292-295.
- [7] L. E. Sanchez-Caldera, "The Mechanism of Corrosion-Erosion in Steam Extract Lines of Power Stations", Ph. D. Thesis, Massachusetts Institute of Technology, Cambridge, Massachusetts (1984).
- [8] W. Kastner and R. Riedle, "Empirisches Modell zur Berechung von Materialabtagen durch Erosionkorrosion", *VGB-Kraftwerkstechnik*, Vol. 66, No. 12, 1986, pp. 1171-1178.
- [9] V. K. Chexal, H. Horowitz, R. Jones, et al., "Flow-Accelerated Corrosion in Power Plants", EPRI TR-106611, Electric Power Research Institute, Palo Alto, 1996.
- [10] K. Yoneda and R. Morita, "Evaluation of Hydraulic Factors Affecting Flow Accelerated Corrosion", <u>Proc. of 13th International Topical Meeting on Nuclear Reactor Thermal Hydraulics (NURETH-13)</u>, N13P1272, Kanazawa, Japan, 2009 Sep. 27 October 2.
- [11] S. Uchida, M. Naitoh, Y. Uehara, H. Okada, T. Ohira, H. Takiguchi, W. Sugino and S. Koshizuka, "Evaluation methods for corrosion damage of components in cooling systems of nuclear power plants by coupling analysis of corrosion and flow dynamics (IV)", *Journal of Nuclear Science and Technology*, Vol. 47, No. 2, 2010, 184-196.
- [12] Y. Utanohara, A. Nakamura, M. Murase and Y. Nagaya, "Measurements of flow field and flow accelerated corrosion in the downstream of an orifice", No. 115, <u>Proc. of the 7th International Topical Meeting on Nuclear Reactor Thermal Hydraulics</u>, <u>Operation and Safety (NUTHOS-7)</u>, Seoul, Korea, 2008 Oct. 5-9.
- [13] Y. Utanohara and A. Nakamura, "RANS prediction of orifice flow and comparison with measurements and LES", Session 15, <u>Proc. of the Second International Conference on Jets, Wakes and Separated Flows (ICJWSF-2008)</u>, Berlin, Germany, 2008 Sep. 16-19.
- [14] Y. Eguchi, T. Murakami, H. Ohshima, H Yamano and S Kotake, "Study on flow-induced-vibration evaluation of large-diameter pipings in a sodium-cooled fast reactor (2) A large-eddy simulation of turbulent flow in a short-elbow pipe", N6P1003, <u>Proc. of 6th Japan-Korea Symposium on Nuclear Thermal Hydraulics and Safety (NTHAS6)</u>, Okinawa, Japan, 2008 Nov. 24-27.